


Communication

In-Site Growth of Efficient NiFeOOH/NiFe-LDH Electrodes: A Streamlined One-Step Methodology

Jing Ning^{1,2,3,†}, Li Xu^{1,2,3,4,†}, Wei Xu⁴, Guizhen Li⁴ and Wen Zhang^{1,2,3,*} 

¹ School of Chemical Engineering and Technology, Tianjin University, Tianjin 300350, China; 2021207014@tju.edu.cn (J.N.); xuli620@tju.edu.cn (L.X.)

² National Industry-Education Integration Platform of Energy Storage, Tianjin University, Tianjin 300350, China

³ Tianjin Key Laboratory of Membrane Science and Desalination Technology, Tianjin 300350, China

⁴ Tianjin Mainland Hydrogen Equipment Co., Ltd., Tianjin 301609, China; xuwei@cnthe.cn (W.X.); liguizhen@cnthe.cn (G.L.)

* Correspondence: zhang_wen@tju.edu.cn

† These authors contributed equally to this work.

Abstract: Oxygen evolution reactions (OER) are often the decisive step in determining the water electrolysis rate. The first row of transition metals and their derivatives, represented by Ni and Fe, have attracted much attention due to their excellent OER performance. Here, we develop a one-step strategy for preparing oxygen-evolving electrodes, in which the NiFeOOH-modified NiFe layered double hydroxide (NiFe-LDH) nanosheet is supported by nickel foam. At 100 mA·cm^{−2}, the overpotential of NiFeOOH-NiFe-LDH was just 227 mV, and the duration times were over 200 h in 1 mol·L^{−1} KOH. Furthermore, the co-existence of LDH and hydroxyl oxides helps the oxygen evolution reaction. These results suggest the potential for this synthesis strategy to provide a low-cost, highly active OER electrocatalyst for industrial water splitting.

Keywords: oxygen evolution reaction; sheet-like nanoarray; NiFeOOH; NiFe-LDH



Citation: Ning, J.; Xu, L.; Xu, W.; Li, G.; Zhang, W. In-Site Growth of Efficient NiFeOOH/NiFe-LDH Electrodes: A Streamlined One-Step Methodology. *Chemistry* **2024**, *6*, 312–322. <https://doi.org/10.3390/chemistry6020017>

Academic Editor: Michael Lyons

Received: 28 February 2024

Revised: 23 March 2024

Accepted: 28 March 2024

Published: 31 March 2024



Copyright: © 2024 by the authors. Licensee MDPI, Basel, Switzerland. This article is an open access article distributed under the terms and conditions of the Creative Commons Attribution (CC BY) license (<https://creativecommons.org/licenses/by/4.0/>).

1. Introduction

Hydrogen energy is a great choice to replace fossil energy because of its advantages of being green, clean, renewable, and easy to transport [1–5]. Among the many ways to produce hydrogen, alkaline electrolytic water is a promising method because of its lower cost and extended stability [6–10]. There are two electrocatalytic reactions, the hydrogen evolution reaction (HER) and oxygen evolution reaction (OER). The OER at the anode side is a four-electron reaction with slow kinetic rates [11–16]. The efficiency of water splitting is mainly dependent on the OER. Therefore, decreasing the OER overpotential becomes the bottleneck to promote the process of alkaline electrolytic water.

The first-row transition metal derivatives, including their oxides [17], hydroxides [18], phosphides [19], sulfides [20], selenides [21] and nitrides [22], have demonstrated a catalytic activity for OER reaction. Many studies have shown that electrodes prepared from the transition metal elements of Ni and Fe have good OER catalytic properties and good prospects for application. In particular, Ni- and Fe-based layered double hydroxides (LDHs) have been considered by many researchers as one of the most promising OER electrodes due to their adjustable electronic configuration, flexible chemical composition, and exchangeable interlayer construction [23–26].

When participating in water electrolysis, the LDH also generates hydroxyl oxides, an intermediate, for the OER catalytic process. Many studies have attempted to prepare hydroxyl oxides as the OER catalysts for efficient electrolytic water. However, the preparation processes of hydroxyl oxides are complicated and often require several reaction steps. Most current preparation methods will first form nano-arrays of metal or metal derivatives on a nickel foam substrate, which are further oxidized to hydroxyl oxides by

anodic electro-oxidation or chemical means [2,27,28]. A phase interface exists between the original nano-arrays and the hydroxyl oxides. The electron transfer across the phase interface is also believed to be a decisive factor in promoting electrolytic water catalysis [2]. Therefore, there is a need to develop novel and simple synthesis strategies for the fabrication of hydroxyl oxides.

In this work, hydroxyl oxide-based OER electrodes were prepared by means of a simple one-step method. NiFeOOH-NiFe-LDH nanosheets were synthesized by immersing nickel foam (NF) in a precursor solution containing nickel ions, iron ions and urea, and heated at 75 °C for 12 h at atmospheric pressure. During this process, the NiFeOOH can be generated on the surface layer of NiFe-LDH supported by NF and accelerate up the OER reaction process. The nanosheets of the two substances are laminated to each other, creating a large number of phase interfaces that help electrons transfer faster. With the overpotential of 0.23 V at 100 mA·cm⁻², the NiFeOOH-NiFe-LDH exhibits remarkable OER efficiency. The electrode also shows good stability, holding steady in 1.0 mol/L KOH for at least 120 h at 200 mA·cm⁻².

2. Materials and Methods

2.1. Materials

The nickel foam (NF) was obtained from Tianjin Leviathan Science & Technology Co., Ltd. (Tianjin, China), with a thickness of 1.0 mm and a porosity of 98%. Ethanol (AR, 99.5%) was purchased from Tianjin Yuanli Chemicals Co., Ltd. (Tianjin, China); Tianjin Hience Optech Technology Company (Tianjin, China) provide Ni(NO₃)₂·6H₂O and CO(NH₂)₂. Shanghai Aladdin Biochemical Technology Co., Ltd. (Shanghai, China) offered Fe(NO₃)₃·9H₂O and KOH. Industrial titanium-based iridium oxide electrodes (Ti/IrO₂) were purchased from Kunshan Yiwanlin Electronic Technology Co., Ltd. (Kushan, China). Analytical grade reagents were utilized as supplied. Deionized water was used to prepare the aqueous solution.

2.2. Materials Synthesis

NF was used to support NiFeOOH-NiFe-LDH nanosheets via a straightforward one-step water bath process. In brief, a 3 cm × 4 cm area of NF was sonicated in 3 mol/L hydrogen chloride (HCl) solution, and deionized water and ethanol were used to remove the surface nickel oxides and organic molecules. To synthesize NiFeOOH-NiFe-LDH/NF, the solution was made by dissolving 178.0 mg Ni(NO₃)₂·6H₂O, 122.4 mg Fe(NO₃)₃·9H₂O (the atomic ratio of Ni: Fe is 2: 1) and 106.2 mg CO(NH₂)₂ in 50 mL deionized water under stirring for 30 min. The cleaned NF was added into this beaker and kept at 75 °C over a period of 12 h. After the sample had completely fallen to room temperature, it was taken out of the beaker. After cooling down to room temperature and washing by deionized water and alcohol, the NiFeOOH-NiFe-LDH was obtained. The sample was dried under 60 °C for 3 h, marked as NiFeOOH-NiFe-LDH.

NiFe-LDH/NF was prepared in the same precursor solution, comprising 178.0 mg Ni(NO₃)₂·6H₂O, 122.4 mg Fe(NO₃)₃·9H₂O and 106.2 mg CO(NH₂)₂ in 50 mL of deionized water. They were kept in a sealed PTFE-lined stainless steel at 120 °C for 12 h. The obtained product was denoted as NiFe-LDH. The empty NF electrode and the purchased industrial Ti/IrO₂ electrode were also used as the control groups.

The synthesis methods for electrodes is illustrated in Figure S1.

2.3. Materials Characterization

The structural information of NiFeOOH-NiFe-LDH were studied by an X-ray diffraction (XRD, Bruker D8, Bruker Corporation, Karlsruhe, Germany). Microstructure and elemental distribution are characterized by scanning electron microstructure (SEM with EDS, Apreo S LoVac, Thermo Fisher Scientific, Hillsboro, Oregon, United States) and transmission electron microscopy (TEM, JEM 2100F, JEOL Ltd., Tokyo, Japan). The chemical state data were obtained via X-ray photoelectron spectroscopy (XPS, Thermo 250Xi, Thermo

Fisher Scientific, Waltham, MA, USA). The composition of substances was further verified by Raman spectroscopy (Raman spectra, Horiba, Horiba Jobin Yvon, Palaiseau, France).

2.4. Electrochemical Measurements

The OER activity in $1 \text{ mol} \cdot \text{L}^{-1}$ KOH was evaluated using an AUTOLAB PGSTAT302N workstation, where NiFe-LDH, NF and Ti/IrO₂ were used directly as the working electrode, and the Hg/HgO was the reference one and the Pt foil electrodes were the counter electrode. Reversible hydrogen electrode (RHE) was used to calibrate the potential. The calibrated equation is $E_{\text{RHE}} = E_{\text{Hg/HgO}} + 0.0591 \times \text{pH} + 0.098 \text{ V}$. In addition, the iR drop of each polarization curve was compensated using an electrochemical workstation.

Linear sweep voltammetry (LSV) was collected under the rate of $5 \text{ mV} \cdot \text{s}^{-1}$. Electrochemical impedance spectroscopy (EIS) was tested at 1.42 V Versus RHE (VRHE) within the frequency from 10^5 Hz to 0.01 Hz with the amplitude of 5 mV . Electrochemical surface areas (ECSA) were studied in a non-Faradic potential window. The potentials were between $1.275 \text{ V}_{\text{RHE}}$ and $1.355 \text{ V}_{\text{RHE}}$ and the scan rates between 40 and $200 \text{ mV} \cdot \text{s}^{-1}$. Chronopotentiometric measurements were made for 120 h at 100 and $200 \text{ mA} \cdot \text{cm}^{-2}$ in order to test durability. The geometric area of the NF was used to normalize the current density.

3. Results

3.1. Structural and Morphological Characterizations of the Electrocatalysts

NiFeOOH-NiFe-LDH prepared in a one-step process was obtained by placing the treated nickel foam directly into a beaker with precursor solution and heating the beaker directly in an oven at 75°C for 12 h (Figure 1). As the temperature rises, the dissolved urea slowly decomposes and breaks down to form an alkaline environment. In the early stage, NiFe-LDH crystals nucleate and grow attached to the nickel foam to form nanosheets. Then, with the decomposition of urea, the metal ions foam hydroxyl oxides attached to nanosheets.

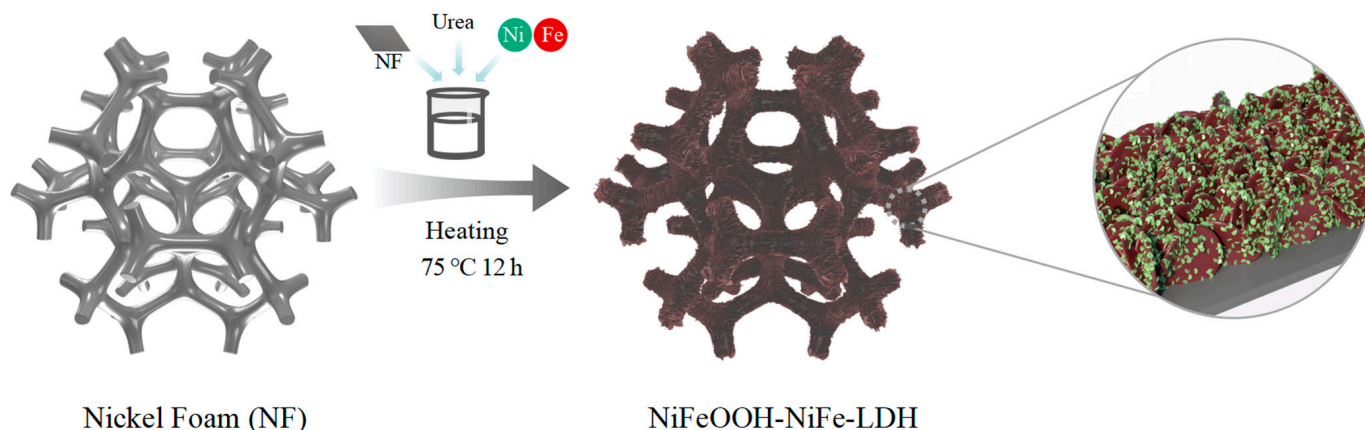


Figure 1. Diagram of the synthesis procedure for H-(Fe_{0.67}Ni_{0.33})OOH-NiFe-LDH/NF.

XRD tests were performed on the NiFeOOH-NiFe-LDH and NiFe-LDH samples attached to nickel foam surface (Figure S2). However, due to the low content of the surface catalytic layer, the diffraction peaks of the catalytic layer cannot be observed. Therefore, the ultrasonic oscillation was used to strip the catalytic layer from nickel foam, and the XRD of exfoliated samples are shown in Figure 2a. The diffraction peaks at 11.4° , 22.9° , 38.9° and 61.2° are the (003), (006), (015) and (113) lattice planes of the NiFe-LDH sample, respectively [23,24]. The diffraction peaks at 34.9° , 40.2° , 53.4° and 62.7° are the (110), (101), (102) and (110) facets of (Fe_{0.67}Ni_{0.33})OOH [28], respectively.

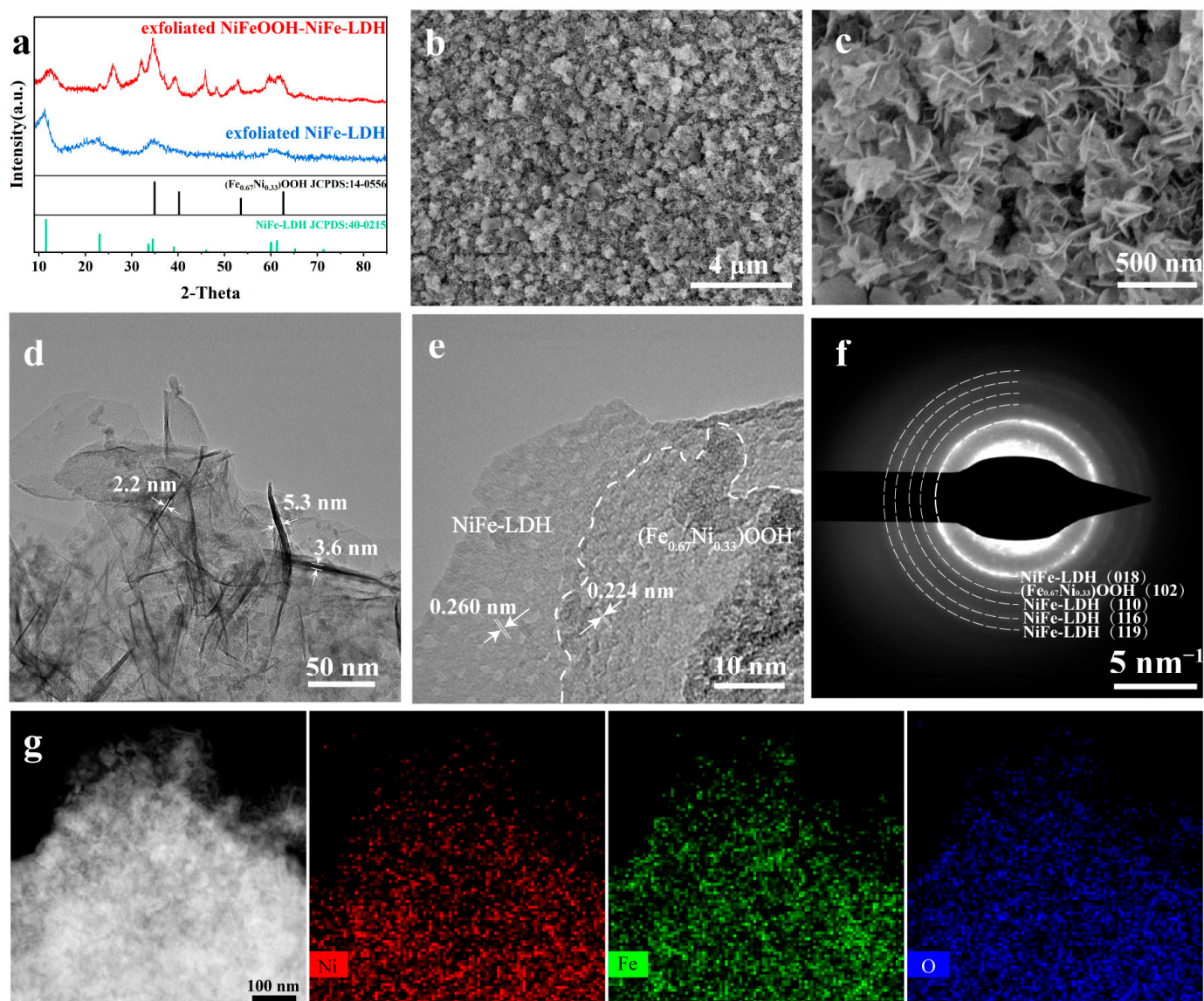


Figure 2. (a) XRD pattern of exfoliated NiFeOOH-NiFe-LDH and exfoliated NiFe-LDH. (b,c) SEM images, (d,e) TEM images, (f) SAED patterns and (g) TEM images with EDS-mapping images of NiFeOOH-NiFe-LDH.

The surface of catalysts was obtained via the SEM. In Figure 2b,c, the SEM images showed that the interconnected ultrathin nanosheets agglomerated into nanocluster structures, growing vertically on the NF surface. The SEM images at low magnification are shown in Figures S3 and S4. The cross-sectional view of the catalyst layer is shown in Figure S5, and the thickness of the NiFeOOH-NiFe-LDH/NF and NiFe-LDH/NF catalyst layers is approximately 3 μm.

The transmission electron microscopy (TEM) images suggest that the nanosheet thickness is thinner, indicating that more reactive sites can be exposed (Figure 2d). In TEM images (Figures 2e and S6), there are visible lattice stripes with the spacing of 0.224 nm, due to the (101) plane of (Fe_{0.67}Ni_{0.33})OOH [28]. The lattice spacing of 0.260 nm is due to the (012) lattice plane of NiFe-LDH [29]. Selected area electron diffraction (SAED) patterns showing diffraction rings (Figure 2f) were also consistent with the above findings. The TEM images and the related EDS mapping (Figure 2g) demonstrated that Ni, Fe and O were uniformly distributed on the nanosheets.

Phase detection was tested using Raman spectroscopy in Figure 3a to verify the substance composition further. The characteristic NiFe-LDH peaks at 453 cm^{-1} and 536 cm^{-1} are due to the vibration of the Ni(II)-O bond in Ni(OH)_2 [30]. The peaks at the corresponding positions in NiFeOOH-NiFe-LDH are 470 cm^{-1} and 544 cm^{-1} , which are considered to be the result of the Ni(III)-O in NiOOH and Ni(II)-O in Ni(OH)_2 [31,32]. Two strong peaks at 308 cm^{-1} and 679 cm^{-1} were detected, corresponding to Fe-O's bending and stretching vibrations in FeOOH, respectively [33,34].

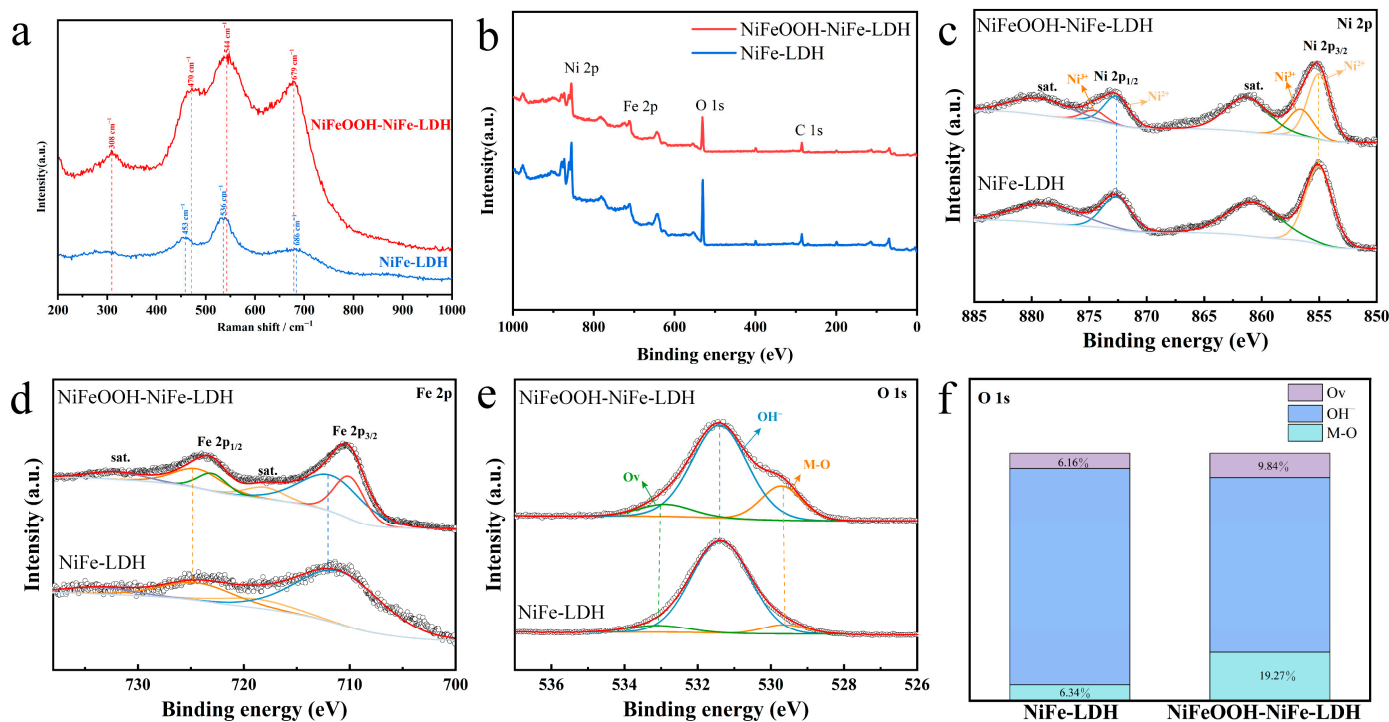


Figure 3. (a) Raman spectra, (b) XPS survey spectra and single-element spectra, (c) Ni 2p, (d) Fe 2p, (e) O 1s and (f) percentage of O element in different forms of NiFeOOH-NiFe-LDH and NiFe-LDH.

XPS was utilized to study compositions of the NiFeOOH-NiFe-LDH and NiFe-LDH samples. In Figure 3b, the XPS reveals the existence of Ni, Fe and O, which is in accordance with EDS mapping images. The prominent Ni 2p peaks in Figure 3c are at 855.3 eV and 872.7 eV, identified as the Ni 2p_{3/2} and Ni 2p_{1/2} peaks, respectively. The typical satellite of Ni 2p_{3/2} and Ni 2p_{1/2} are the broad peaks at 861.4 and 879.7 eV [35]. The Ni 2p peak fitting analysis indicates the existence of two states of Ni 2p, $\text{Ni}^{2+}(t_{2g}^6 e_g^2)$ and $\text{Ni}^{3+}(t_{2g}^6 e_g^1)$, which can be attributed to Ni species in Ni(OH)_2 and NiOOH, respectively. It is shown in Figure S7 that the prepared sample NiFeOOH-NiFe-LDH contains a high percentage of Ni^{3+} (30.8%). Many reports have shown that the introduction of high-valent Ni can effectively enhance the electron-withdrawing effect, and the electronic configuration of $\text{Ni}^{3+}(t_{2g}^6 e_g^1)$ is more favorable to the OER by forming σ -bonds with adsorbed oxygen [11,36].

Fe 2p in Figure 3d shows the peaks of NiFeOOH-NiFe-LDH at 710.3 eV and 723.6 eV, with the satellites at 717.0 eV and 732.6 eV, corresponding to the Fe 2p_{3/2} and Fe 2p_{1/2}, respectively. The peak fitting of NiFeOOH-NiFe-LDH suggests that Fe^{3+} exists in different compositions. The peak located at 712.1 eV is attributed to FeOOH, and the peak at 710.2 eV is attributed to Fe(OH)_3 . These results agree with the finding of XRD [37–39].

The split-peak fitting of the O 1s spectra in Figure 3e shows that the lattice oxygen (M-O) is at 529.6 eV, the metal hydroxide (M-OH) is at 531.4 eV and the oxygen vacancy (Ov) is at 533.1 eV. It is clear from Figure 3f that the percentage of M-O of NiFeOOH-NiFe-LDH is considerably higher than the percentage of NiFe-LDH, suggesting the generation of hydroxyl oxides in NiFeOOH-NiFe-LDH.

NiFeOOH-NiFe-LDH has more oxygen vacancies than NiFe-LDH (Figure S5), suggesting the presence of high valence Ni in NiFeOOH-NiFe-LDH, which is beneficial to the OER reaction [40,41].

3.2. Electrochemical Test Performance

By means of a three-electrode setup, we investigated the electrochemical OER performance of various electrodes in 1 mol·L⁻¹ KOH solution. Commercial IrO₂/Ti and NF were also tested for comparison. In Figure 4a, the onset potential of NiFeOOH-NiFe-LDH at 1 mA·cm⁻² was 1.337 V. NiFeOOH-NiFe-LDH has an overpotential of only 227 mV at 100 mA·cm⁻², which was not only the lowest overpotential among the electrodes (Figure 4b) but also better than recently reported catalysts (Table 1).

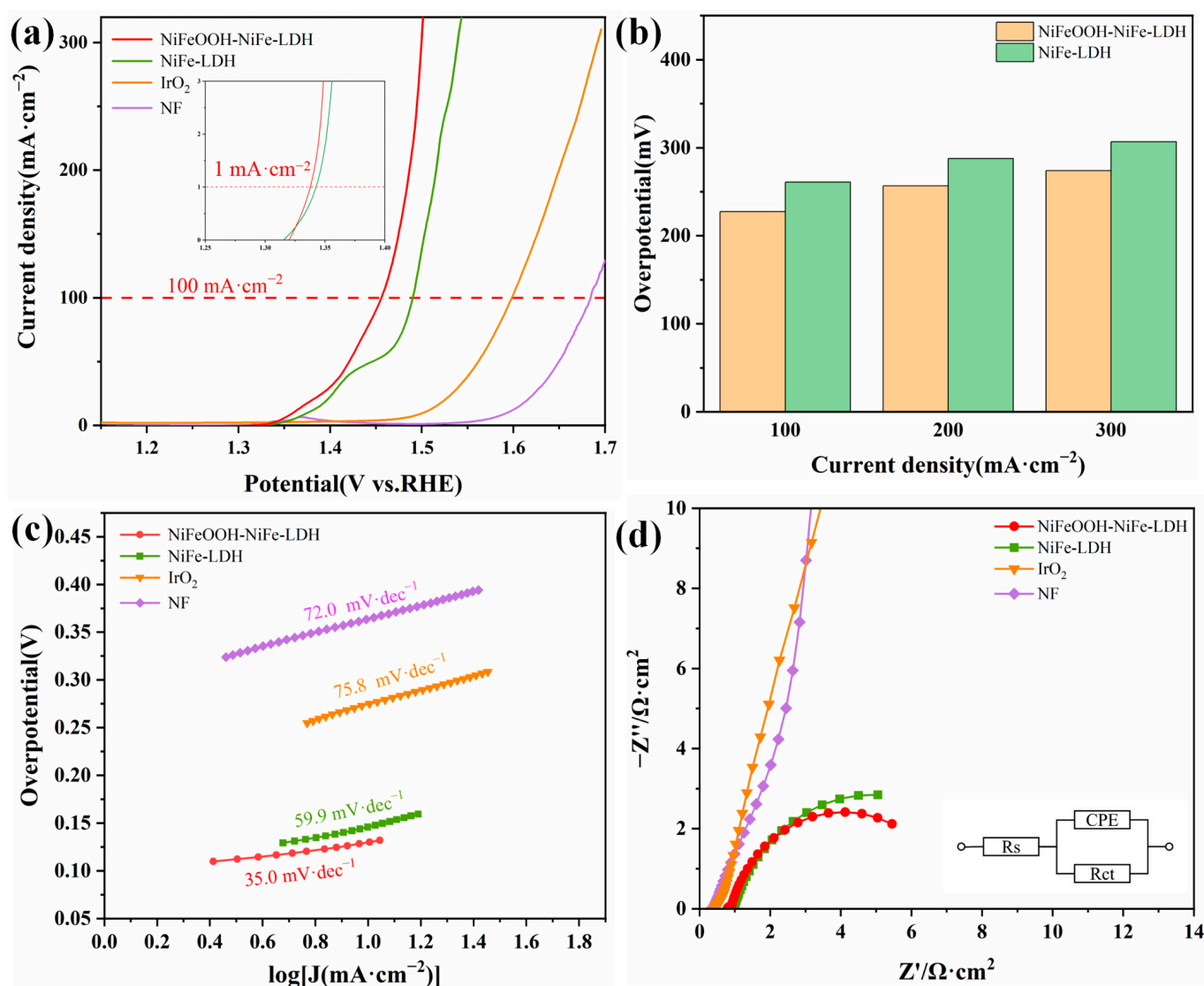


Figure 4. Electrochemical performance of various catalysts in 1 mol·L⁻¹ KOH. (a) Polarization curves. (b) The overpotentials required for current density of 100, 200 and 300 mA·cm⁻². (c) Tafel plots. (d) Nyquist plots at 1.425 V_{RHE}.

Additionally, the kinetic of electrodes was evaluated by calculating the Tafel curves based on the polarization curves. In Figure 4c, NiFeOOH-NiFe-LDH has the fastest OER reaction kinetics and lowest Tafel slope of 35.0 mV·dec⁻¹. The enhanced kinetics are verified by the electrochemical impedance (Figure 4d) characterization, with the charge transfer

resistance (R_{ct}) of NiFeOOH-NiFe-LDH being the lowest among all of these samples ($6.343 \Omega \cdot \text{cm}^2$, Table 2).

Table 1. Comparison of OER performances between NiFeOOH-NiFe-LDH electrode and recently reported electrocatalysts in alkaline solution.

Catalyst	Substrate	Overpotential (mV)	Tafel Slope (mV dec ⁻¹)	Stability	Ref.
NiFeOOH-NiFe-LDH	^a NF	227@100 mA cm ⁻²	35.0	120 h@200 mA cm ⁻²	
NiFe-LDH-NS	^b DG	210@10 mA cm ⁻²	52.0	10 h@10 mA cm ⁻²	[42]
NiFe-LDH	^c GCE	270@10 mA cm ⁻²	-	24 h@10 mA cm ⁻²	[37]
Mesoporous NiO/NiFe ₂ O ₄	GCE	302@10 mA cm ⁻²	42	2 h @20 mA cm ⁻²	[43]
FeP _x /Fe-N-C/NPC	NF	325@10 mA cm ⁻²	79	24 h@10 mA cm ⁻²	[44]
Fe-NiO/NF	NF	264, 336@10, 100 mA cm ⁻²	65.3	12 h@60 mA cm ⁻²	[45]
N-NiMoO ₄ /NiS ₂	^d CF	267, 335@10, 100 mA cm ⁻²	-	-	[46]
N-CNTs@NiS ₂ /Fe ₇ S ₈	GCE	330@50 mA cm ⁻²	51.49	24 h@50 mA cm ⁻²	[47]
Amorphous (Fe-Ni)Co _x -OH/Ni ₃ S ₂	NF	280@100 mA cm ⁻²	57	100 h@200 mA cm ⁻²	[48]
NiFeCo-LDH	^e RDE	249@10 mA cm ⁻²	46	80 h@100 mA cm ⁻²	[49]
Co@NiFe-LDH	RDE	253@10 mA cm ⁻²	44	50 h@10 mA cm ⁻²	[50]
Ni ₄ FeW-LDH	^f CP	248@20 mA cm ⁻²	68	6 h@10 mA cm ⁻²	[51]
Cr/FeNi-LDH	^g SS	202, 242@10, 100 mA cm ⁻²	32.5	15 h@10 mA cm ⁻²	[52]
FeOOH-NiCoMo-LDH	NF	252@50 mA cm ⁻²	59.39	50 h@50 mA cm ⁻²	[53]
S-NiMoO ₄ @NiFe-LDH	NF	273@100 mA cm ⁻²	90	20 h@60 mA cm ⁻²	[17]
NiFe(OH) _x /Ni ₃ N	NF	260@10 mA cm ⁻²	35	-	[54]
NiFeOx-LDH	GEC	227@10 mA cm ⁻²	54	20 h@100 mA cm ⁻²	[55]
Ru-NiFe-LDH	CC	246@10 mA cm ⁻²	67.2	6 h@10 mA cm ⁻²	[38]

^a NF; nickel foam, ^b DG; defective graphene, ^c GCE; glassy carbon electrode, ^d CF; carbon fiber, ^e RDE; glassy carbon electrode, ^f CP; carbon paper, ^g SS; stainless steel. All electrochemical tests were conducted in 1.0 M KOH except for Ref [14] (1.0 M KOH + 0.5 M NaCl freshwater).

Table 2. Equivalent circuit used for EIS data analysis and summary of the parameters obtained from various as-prepared electrodes.

Samples	R_s (Ω)	R_{ct} (Ω)	CPE.Y0 (F)	CPE.N
NiFeOOH-NiFe-LDH	0.9088	6.3429	1.1096	0.8192
NiFe-LDH	0.9400	8.6666	1.8364	0.7585
IrO ₂	0.8736	219.51	0.0725	0.8728
Nickel Foam	2.7036	1321.4	0.0120	0.9700

CV curves based on the non-Faraday region of 1.275 V–1.355 V vs. RHE were calculated from the ECSA (Figure 5a–d, Table S1). In this way, the corresponding double-layer capacitance (C_{dl}) can be calculated for different catalysts. In particular, the C_{dl} of NiFeOOH-NiFe-LDH is $7.19 \text{ mF} \cdot \text{cm}^{-2}$, more significant than those of the other electrodes (Figure 5e). In comparison to NiFe-LDH, the surface area of NiFeOOH-NiFe-LDH is effectively increased. In $1 \text{ mol} \cdot \text{L}^{-1}$ KOH, stability tests of NiFeOOH-NiFe-LDH were conducted at $100 \text{ mA} \cdot \text{cm}^{-2}$ for 200 h (Figure 5f). It is observed that even after 200 h, the catalytic activity of NiFeOOH-NiFe-LDH remains at a high level, demonstrating its remarkable stability. The excellent catalytic activity of NiFeOOH-NiFe-LDH can be attributed to NiFeOOH serving as an intermediate in the OER mechanism, which promotes faster reaction rates.

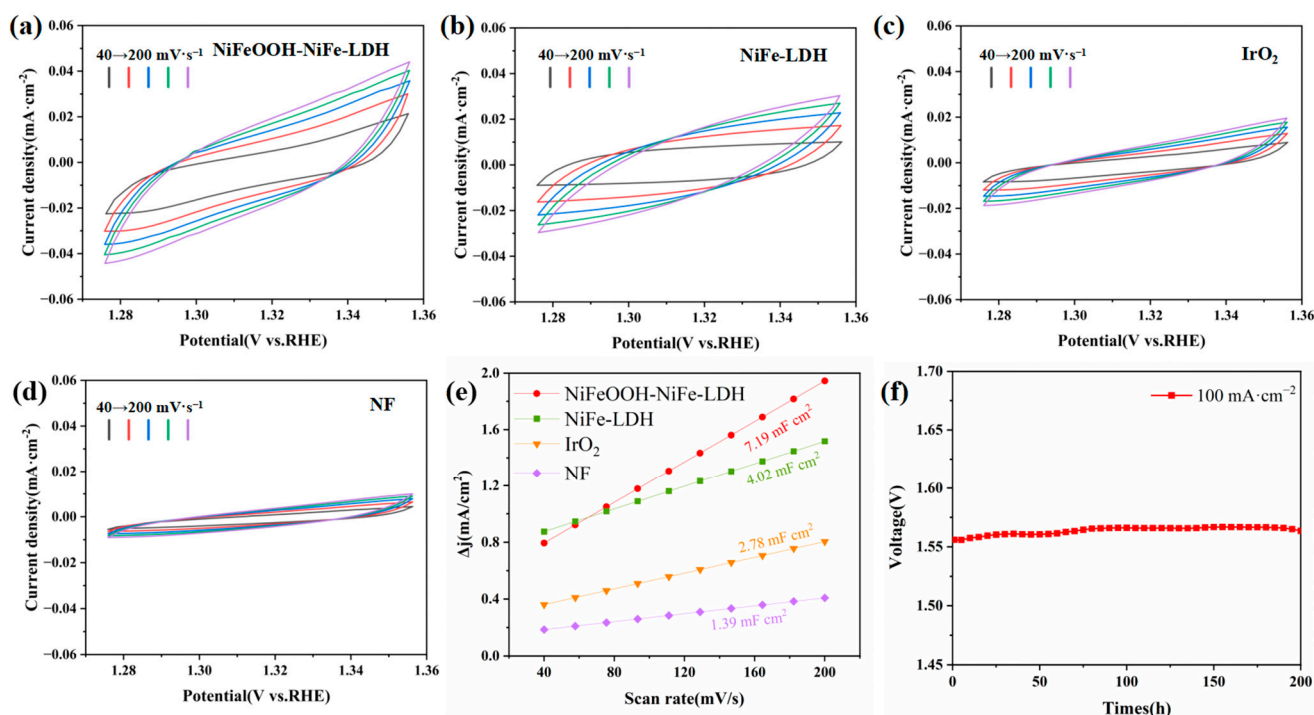


Figure 5. The Cdl measurement at the non-Faraday region potential window: (a) NiFeOOH-NiFe-LDH, (b) NiFe-LDH, (c) IrO₂ and (d) NF. (e) The value of Cdl of different catalysts. (f) Chronoamperometric plots at 100 mA·cm⁻² for NiFeOOH-NiFe-LDH.

4. Conclusions

In this study, we explored a strategy to prepare the NiFeOOH/NiFe-LDH electrode by in-site growth of NiFeOOH-decorated NiFe-LDH nanosheets on NF support and compared it with NiFe-LDH (Table S2). Mechanistic analysis showed that the presence of the reaction intermediate NiFeOOH promoted the rapid occurrence of OER. The prepared NiFeOOH-NiFe-LDH has a low overpotential of 227 mV while providing 100 mA·cm⁻² current density. It also has a durability of up to 120 h in operation at 200 mA·cm⁻². The outstanding electrochemical performance can be attributed to its unique composition and nanostructure and the abundance of phase interfaces that enhance the exposure of catalytically active sites. This work provides a new strategy for preparing NiFe-based electrodes for OER reactions.

Supplementary Materials: The following supporting information can be downloaded at: <https://www.mdpi.com/article/10.3390/chemistry6020017/s1>. Figure S1: synthesis methods for experimental electrodes; Figure S2: SEM images of NF; Figure S3: (a) SEM images and (b) TEM image of NiFe-LDH/NF; Figure S4: calculation of lattice stripes corresponding to two phase frame selection positions; Figure S5: percentage of Ni²⁺ and Ni³⁺ of NiFeOOH-NiFe-LDH; Figure S6: Calculation of lattice stripes corresponding to two phase frame selection positions; Figure S7: Percentage of Ni²⁺ and Ni³⁺ of NiFeOOH-NiFe-LDH; Table S1: The ECSA and Cdl values of different catalysts; Table S2: The comparisons between NiFeOOH-NiFe-LDH and NiFe-LDH.

Author Contributions: Conceptualization, J.N. and W.Z.; methodology, J.N., L.X. and W.X.; Validation, J.N. and L.X. and G.L.; formal analysis, J.N. and L.X.; investigation, J.N., L.X. and G.L.; resources, G.L. and W.X.; data curation, J.N.; writing—original draft preparation, J.N. and L.X.; writing—review and editing, W.Z.; visualization, J.N., G.L. and W.X.; supervision, W.Z. and L.X.; project administration, L.X.; funding acquisition, L.X. All authors have read and agreed to the published version of the manuscript.

Funding: This research was funded by the National Key R&D Program (No. 2021YFB4000303).

Data Availability Statement: The data presented in this study are available on request from the corresponding author. The data are not publicly available due to further research is being carried out.

Conflicts of Interest: Authors L.X., W.X. and G.L. were employed by company Tianjin Mainland Hydrogen Equipment Co., Ltd. The remaining authors declare that the research was conducted in the absence of any commercial or financial relationships that could be construed as a potential conflict of interest.

References

1. Zhao, M.; Wang, Y.; Mi, W.; Wu, J.; Zou, J.-J.; Zhu, X.-D.; Gao, J.; Zhang, Y.-C. Surface-modified amorphous FeOOH on NiFe LDHs for high efficiency electrocatalytic oxygen evolution. *Electrochim. Acta* **2023**, *458*, 142513. [\[CrossRef\]](#)
2. Liang, Y.; Wang, J.; Liu, D.; Wu, L.; Li, T.; Yan, S.; Fan, Q.; Zhu, K.; Zou, Z. Ultrafast Fenton-like reaction route to FeOOH/NiFe-LDH heterojunction electrode for efficient oxygen evolution reaction. *J. Mater. Chem. A* **2021**, *9*, 21785–21791. [\[CrossRef\]](#)
3. Wan, Z.; Ma, Z.; Yuan, H.; Liu, K.; Wang, X. Sulfur Engineering on NiFe Layered Double Hydroxide at Ambient Temperature for High Current Density Oxygen Evolution Reaction. *ACS Appl. Energy Mater.* **2022**, *5*, 4603–4612. [\[CrossRef\]](#)
4. Luo, Y.; Wu, Y.; Wu, D.; Huang, C.; Xiao, D.; Chen, H.; Zheng, S.; Chu, P.K. NiFe-Layered Double Hydroxide Synchronously Activated by Heterojunctions and Vacancies for the Oxygen Evolution Reaction. *ACS Appl. Mater. Interfaces* **2020**, *12*, 42850–42858. [\[CrossRef\]](#)
5. Xu, L.; Dong, Y.; Xu, W.; Zhang, W. Ultrafast and Facile Synthesis of (Ni/Fe/Mo)OOH on Ni Foam for Oxygen Evolution Reaction in Seawater Electrolysis. *Catalysts* **2023**, *13*, 924. [\[CrossRef\]](#)
6. Zeng, K.; Zhang, D. Recent progress in alkaline water electrolysis for hydrogen production and applications. *Prog. Energy Combust. Sci.* **2010**, *36*, 307–326. [\[CrossRef\]](#)
7. Dong, Z.-H.; Jiang, Z.; Tang, T.; Yao, Z.-C.; Xue, D.; Niu, S.; Zhang, J.; Hu, J.-S. Rational design of integrated electrodes for advancing high-rate alkaline electrolytic hydrogen production. *J. Mater. Chem. A* **2022**, *10*, 12764–12787. [\[CrossRef\]](#)
8. Chi, J.; Yu, H. Water electrolysis based on renewable energy for hydrogen production. *Chin. J. Catal.* **2018**, *39*, 390–394. [\[CrossRef\]](#)
9. Xu, L.; Yuan, B.; Min, L.; Xu, W.; Zhang, W. Preparation of NiCo-LDH@NiCoV-LDH interconnected nanosheets as high-performance electrocatalysts for overall water splitting. *Int. J. Hydrogen Energy* **2022**, *47*, 15583–15592. [\[CrossRef\]](#)
10. Chen, Y.; Min, L.; Zhang, W.; Xu, L.; Wang, Y. Crown ether as a bifunctional booster in electrochemical water splitting. *Int. J. Hydrogen Energy* **2024**, *51*, 1534–1543. [\[CrossRef\]](#)
11. Wang, Z.; Liu, W.; Hu, Y.; Guan, M.; Xu, L.; Li, H.; Bao, J.; Li, H. Cr-doped CoFe layered double hydroxides: Highly efficient and robust bifunctional electrocatalyst for the oxidation of water and urea. *Appl. Catal. B Environ.* **2020**, *272*, 118959. [\[CrossRef\]](#)
12. Zhang, X.-P.; Wang, H.-Y.; Zheng, H.; Zhang, W.; Cao, R. O–O bond formation mechanisms during the oxygen evolution reaction over synthetic molecular catalysts. *Chin. J. Catal.* **2021**, *42*, 1253–1268. [\[CrossRef\]](#)
13. Zhang, Z.; Li, X.; Zhong, C.; Zhao, N.; Deng, Y.; Han, X.; Hu, W. Spontaneous Synthesis of Silver-Nanoparticle-Decorated Transition-Metal Hydroxides for Enhanced Oxygen Evolution Reaction. *Angew. Chem. Int. Ed. Engl.* **2020**, *59*, 7245–7250. [\[CrossRef\]](#)
14. Chen, Z.; Qu, Q.; Li, X.; Srinivas, K.; Chen, Y.; Zhu, M. Room-Temperature Synthesis of Carbon-Nanotube-Interconnected Amorphous NiFe-Layered Double Hydroxides for Boosting Oxygen Evolution Reaction. *Molecules* **2023**, *28*, 7289. [\[CrossRef\]](#)
15. Liu, Q.; Wang, Y.; Lu, X. Construction of NiFe-Layered Double Hydroxides Arrays as Robust Electrocatalyst for Oxygen Evolution Reaction. *Catalysts* **2023**, *13*, 586. [\[CrossRef\]](#)
16. Guo, D.; Chi, J.; Yu, H.; Jiang, G.; Shao, Z. Self-Supporting NiFe Layered Double Hydroxide “Nanoflower” Cluster Anode Electrode for an Efficient Alkaline Anion Exchange Membrane Water Electrolyzer. *Energies* **2022**, *15*, 4645. [\[CrossRef\]](#)
17. Wang, H.; Chen, L.; Tan, L.; Liu, X.; Wen, Y.; Hou, W.; Zhan, T. Electrodeposition of NiFe-layered double hydroxide layer on sulfur-modified nickel molybdate nanorods for highly efficient seawater splitting. *J. Colloid Interface Sci.* **2022**, *613*, 349–358. [\[CrossRef\]](#)
18. Ma, Y.; Wang, Y.; Xie, D.; Gu, Y.; Zhang, H.; Wang, G.; Zhang, Y.; Zhao, H.; Wong, P.K. NiFe-Layered Double Hydroxide Nanosheet Arrays Supported on Carbon Cloth for Highly Sensitive Detection of Nitrite. *ACS Appl. Mater. Interfaces* **2018**, *10*, 6541–6551. [\[CrossRef\]](#)
19. Lai, D.; Kang, Q.; Gao, F.; Lu, Q. High-entropy effect of a metal phosphide on enhanced overall water splitting performance. *J. Mater. Chem. A* **2021**, *9*, 17913–17922. [\[CrossRef\]](#)
20. Zhao, C.-X.; Li, B.-Q.; Zhao, M.; Liu, J.-N.; Zhao, L.-D.; Chen, X.; Zhang, Q. Precise anionic regulation of NiFe hydroxysulfide assisted by electrochemical reactions for efficient electrocatalysis. *Energy Environ. Sci.* **2020**, *13*, 1711–1716. [\[CrossRef\]](#)
21. Zhou, T.; Bai, J.; Gao, Y.; Zhao, L.; Jing, X.; Gong, Y. Selenide-based 3D folded polycrystalline nanosheets for a highly efficient oxygen evolution reaction. *J. Colloid Interface Sci.* **2022**, *615*, 256–264. [\[CrossRef\]](#) [\[PubMed\]](#)
22. Jia, X.; Zhao, Y.; Chen, G.; Shang, L.; Shi, R.; Kang, X.; Waterhouse, G.I.N.; Wu, L.-Z.; Tung, C.-H.; Zhang, T. Ni₃FeN Nanoparticles Derived from Ultrathin NiFe-Layered Double Hydroxide Nanosheets: An Efficient Overall Water Splitting Electrocatalyst. *Adv. Energy Mater.* **2016**, *6*, 1502585. [\[CrossRef\]](#)
23. Bodhankar, P.M.; Sarawade, P.B.; Singh, G.; Vinu, A.; Dhawale, D.S. Recent advances in highly active nanostructured NiFe LDH catalyst for electrochemical water splitting. *J. Mater. Chem. A* **2021**, *9*, 3180–3208. [\[CrossRef\]](#)

24. Ding, P.; Meng, C.; Liang, J.; Li, T.; Wang, Y.; Liu, Q.; Luo, Y.; Cui, G.; Asiri, A.M.; Lu, S.; et al. NiFe Layered-Double-Hydroxide Nanosheet Arrays on Graphite Felt: A 3D Electrocatalyst for Highly Efficient Water Oxidation in Alkaline Media. *Inorg. Chem.* **2021**, *60*, 12703–12708. [\[CrossRef\]](#) [\[PubMed\]](#)
25. Chen, R.; Hung, S.F.; Zhou, D.; Gao, J.; Yang, C.; Tao, H.; Yang, H.B.; Zhang, L.; Zhang, L.; Xiong, Q.; et al. Layered Structure Causes Bulk NiFe Layered Double Hydroxide Unstable in Alkaline Oxygen Evolution Reaction. *Adv. Mater.* **2019**, *31*, e1903909. [\[CrossRef\]](#) [\[PubMed\]](#)
26. Feng, X.; Jiao, Q.; Chen, W.; Dang, Y.; Dai, Z.; Suib, S.L.; Zhang, J.; Zhao, Y.; Li, H.; Feng, C. Cactus-like NiCo₂S₄@NiFe LDH hollow spheres as an effective oxygen bifunctional electrocatalyst in alkaline solution. *Appl. Catal. B Environ.* **2021**, *286*, 119869. [\[CrossRef\]](#)
27. Lin, Z.; Bu, P.; Xiao, Y.; Gao, Q.; Diao, P. β - and γ -NiFeOOH electrocatalysts for an efficient oxygen evolution reaction: An electrochemical activation energy aspect. *J. Mater. Chem. A* **2022**, *10*, 20847–20855. [\[CrossRef\]](#)
28. Wang, M.; Cao, K.; Tian, Z.; Sheng, P. Increased charge and mass transfer derived-sheet-like Fe_{0.67}Ni_{0.33}OOH-Fe₂O₃@NF array for robust oxygen evolution reaction. *Appl. Surf. Sci.* **2019**, *493*, 351–358. [\[CrossRef\]](#)
29. Dang, Y.; Li, X.; Chen, Z.; Zhao, X.; Ma, B.; Chen, Y. Hierarchical MoN@NiFe-LDH Heterostructure Nanowire Array for Highly Efficient Electrocatalytic Hydrogen Evolution. *Small* **2023**, *19*, e2303932. [\[CrossRef\]](#)
30. Li, Y.; Wu, Y.; Yuan, M.; Hao, H.; Lv, Z.; Xu, L.; Wei, B. Operando spectroscopies unveil interfacial FeOOH induced highly reactive β -Ni(Fe)OOH for efficient oxygen evolution. *Appl. Catal. B Environ.* **2022**, *318*, 121825. [\[CrossRef\]](#)
31. Durr, R.N.; Maltoni, P.; Tian, H.; Joussetme, B.; Hammarstrom, L.; Edvinsson, T. From NiMoO(4) to gamma-NiOOH: Detecting the Active Catalyst Phase by Time Resolved in Situ and Operando Raman Spectroscopy. *ACS Nano* **2021**, *15*, 13504–13515. [\[CrossRef\]](#)
32. Yan, P.; Liu, Q.; Zhang, H.; Qiu, L.; Wu, H.B.; Yu, X.-Y. Deeply reconstructed hierarchical and defective NiOOH/FeOOH nanoboxes with accelerated kinetics for the oxygen evolution reaction. *J. Mater. Chem. A* **2021**, *9*, 15586–15594. [\[CrossRef\]](#)
33. Luo, W.; Jiang, C.; Li, Y.; Shevlin, S.A.; Han, X.; Qiu, K.; Cheng, Y.; Guo, Z.; Huang, W.; Tang, J. Highly crystallized α -FeOOH for a stable and efficient oxygen evolution reaction. *J. Mater. Chem. A* **2017**, *5*, 2021–2028. [\[CrossRef\]](#)
34. Chemelewski, W.D.; Lee, H.C.; Lin, J.F.; Bard, A.J.; Mullins, C.B. Amorphous FeOOH oxygen evolution reaction catalyst for photoelectrochemical water splitting. *J. Am. Chem. Soc.* **2014**, *136*, 2843–2850. [\[CrossRef\]](#)
35. Wang, F.-L.; Yu Zhang, X.; Zhou, J.-C.; Shi, Z.-N.; Dong, B.; Xie, J.-Y.; Dong, Y.-W.; Yu, J.-F.; Chai, Y.-M. Amorphous–crystalline FeNi₂S₄@NiFe–LDH nanograsses with molten salt as an industrially promising electrocatalyst for oxygen evolution. *Inorg. Chem. Front.* **2022**, *9*, 2068–2080. [\[CrossRef\]](#)
36. Zhai, Y.; Ren, X.; Sun, Y.; Li, D.; Wang, B.; Liu, S. Synergistic effect of multiple vacancies to induce lattice oxygen redox in NiFe-layered double hydroxide OER catalysts. *Appl. Catal. B Environ.* **2023**, *323*, 122091. [\[CrossRef\]](#)
37. Suliman, M.; Al Ghamdi, A.; Baroud, T.; Drmash, Q.; Rafatullah, M.; Yamani, Z.; Qamar, M. Growth of ultrathin nanosheets of nickel iron layered double hydroxide for the oxygen evolution reaction. *Int. J. Hydrogen Energy* **2022**, *47*, 23498–23507. [\[CrossRef\]](#)
38. Yang, Y.; Wang, W.-J.; Yang, Y.-B.; Guo, P.-F.; Zhu, B.; Wang, K.; Wang, W.-T.; He, Z.-H.; Liu, Z.-T. Ru-Doped NiFe Layered Double Hydroxide as a Highly Active Electrocatalyst for Oxygen Evolution Reaction. *J. Electrochem. Soc.* **2022**, *169*, 024503. [\[CrossRef\]](#)
39. Biesinger, M.C.; Payne, B.P.; Grosvenor, A.P.; Lau, L.W.M.; Gerson, A.R.; Smart, R.S.C. Resolving surface chemical states in XPS analysis of first row transition metals, oxides and hydroxides: Cr, Mn, Fe, Co and Ni. *Appl. Surf. Sci.* **2011**, *257*, 2717–2730. [\[CrossRef\]](#)
40. Wang, Y.; Tao, S.; Lin, H.; Wang, G.; Zhao, K.; Cai, R.; Tao, K.; Zhang, C.; Sun, M.; Hu, J.; et al. Atomically targeting NiFe LDH to create multivacancies for OER catalysis with a small organic anchor. *Nano Energy* **2021**, *81*, 105606. [\[CrossRef\]](#)
41. Wu, B.; Gong, S.; Lin, Y.; Li, T.; Chen, A.; Zhao, M.; Zhang, Q.; Chen, L. A Unique NiOOH@FeOOH Heteroarchitecture for Enhanced Oxygen Evolution in Saline Water. *Adv. Mater.* **2022**, *34*, e2108619. [\[CrossRef\]](#)
42. Jia, Y.; Zhang, L.; Gao, G.; Chen, H.; Wang, B.; Zhou, J.; Soo, M.T.; Hong, M.; Yan, X.; Qian, G.; et al. A Heterostructure Coupling of Exfoliated Ni–Fe Hydroxide Nanosheet and Defective Graphene as a Bifunctional Electrocatalyst for Overall Water Splitting. *Adv. Mater.* **2017**, *29*, 1700017. [\[CrossRef\]](#)
43. Liu, G.; Gao, X.; Wang, K.; He, D.; Li, J. Uniformly mesoporous NiO/NiFe₂O₄ biphasic nanorods as efficient oxygen evolving catalyst for water splitting. *Int. J. Hydrogen Energy* **2016**, *41*, 17976–17986. [\[CrossRef\]](#)
44. Qin, Q.; Jang, H.; Li, P.; Yuan, B.; Liu, X.; Cho, J. A Tannic Acid-Derived N-, P-Codoped Carbon-Supported Iron-Based Nanocomposite as an Advanced Trifunctional Electrocatalyst for the Overall Water Splitting Cells and Zinc-Air Batteries. *Adv. Energy Mater.* **2019**, *9*, 1803312. [\[CrossRef\]](#)
45. Qiu, Z.; Ma, Y.; Edvinsson, T. In operando Raman investigation of Fe doping influence on catalytic NiO intermediates for enhanced overall water splitting. *Nano Energy* **2019**, *66*, 104118. [\[CrossRef\]](#)
46. An, L.; Feng, J.; Zhang, Y.; Wang, R.; Liu, H.; Wang, G.-C.; Cheng, F.; Xi, P. Epitaxial Heterogeneous Interfaces on N-NiMoO₄/NiS₂ Nanowires/Nanosheets to Boost Hydrogen and Oxygen Production for Overall Water Splitting. *Adv. Funct. Mater.* **2019**, *29*, 1805298. [\[CrossRef\]](#)
47. Wang, J.-Y.; Liu, W.-T.; Li, X.-P.; Ouyang, T.; Liu, Z.-Q. Strong hydrophilicity NiS₂/Fe₇S₈ heterojunctions encapsulated in N-doped carbon nanotubes for enhanced oxygen evolution reaction. *Chem. Commun.* **2020**, *56*, 1489–1492. [\[CrossRef\]](#)
48. Che, Q.; Li, Q.; Chen, X.; Tan, Y.; Xu, X. Assembling amorphous (Fe-Ni)Co-OH/Ni₃S₂ nanohybrids with S-vacancy and interfacial effects as an ultra-highly efficient electrocatalyst: Inner investigation of mechanism for alkaline water-to-hydrogen/oxygen conversion. *Appl. Catal. B Environ.* **2020**, *263*, 118338. [\[CrossRef\]](#)

49. Park, Y.S.; Jeong, J.-Y.; Jang, M.J.; Kwon, C.-Y.; Kim, G.H.; Jeong, J.; Lee, J.-H.; Lee, J.; Choi, S.M. Ternary layered double hydroxide oxygen evolution reaction electrocatalyst for anion exchange membrane alkaline seawater electrolysis. *J. Energy Chem.* **2022**, *75*, 127–134. [[CrossRef](#)]
50. Liu, S.; Wan, R.; Lin, Z.; Liu, Z.; Liu, Y.; Tian, Y.; Qin, D.-D.; Tang, Z. Probing the Co role in promoting the OER and Zn–air battery performance of NiFe-LDH: A combined experimental and theoretical study. *J. Mater. Chem. A* **2022**, *10*, 5244–5254. [[CrossRef](#)]
51. Guo, P.-F.; Yang, Y.; Wang, W.-J.; Zhu, B.; Wang, W.-T.; Wang, Z.-Y.; Wang, J.-L.; Wang, K.; He, Z.-H.; Liu, Z.-T. Stable and active NiFeW layered double hydroxide for enhanced electrocatalytic oxygen evolution reaction. *Chem. Eng. J.* **2021**, *426*, 130768. [[CrossRef](#)]
52. Xie, X.; Cao, C.; Wei, W.; Zhou, S.; Wu, X.-T.; Zhu, Q.-L. Ligand-assisted capping growth of self-supporting ultrathin FeNi-LDH nanosheet arrays with atomically dispersed chromium atoms for efficient electrocatalytic water oxidation. *Nanoscale* **2020**, *12*, 5817–5823. [[CrossRef](#)] [[PubMed](#)]
53. Luo, H.; Liang, J.; Zhou, J.; Yin, Z.; Zhang, Z.; Liu, X. Synergistic coupling of FeOOH with Mo-incorporated NiCo LDH towards enhancing the oxygen evolution reaction. *New J. Chem.* **2022**, *46*, 7999–8009. [[CrossRef](#)]
54. Zhang, H.; Meng, X.; Zhang, J.; Huang, Y. Hierarchical NiFe Hydroxide/Ni₃N Nanosheet-on-Nanosheet Heterostructures for Bifunctional Oxygen Evolution and Urea Oxidation Reactions. *ACS Sustain. Chem. Eng.* **2021**, *9*, 12584–12590. [[CrossRef](#)]
55. Xu, X.; Wang, T.; Zheng, M.; Li, Y.; Shi, J.; Tian, T.; Jia, R.; Liu, Y. Metal-organic framework assisted formation of Ni-Fe-based porous nanoflowers for enhanced water splitting. *J. Alloys Compd.* **2021**, *875*, 159970. [[CrossRef](#)]

Disclaimer/Publisher’s Note: The statements, opinions and data contained in all publications are solely those of the individual author(s) and contributor(s) and not of MDPI and/or the editor(s). MDPI and/or the editor(s) disclaim responsibility for any injury to people or property resulting from any ideas, methods, instructions or products referred to in the content.